

Geometrical Effects of the Discharge System on the Corona Discharge and Chemically Active Species Generated in Wire-Cylinder and Wire-Plate Reactors

Yongho KIM,* Jin Myung PARK and Sang Hee HONG

Department of Nuclear Engineering, Seoul National University, Seoul 151-742

(Received 20 November 2003)

Time-dependent one- and two-dimensional numerical models are developed to analyze the influence of the design and the operating conditions on streamer propagation and active-species generation in wire-cylinder and wire-plate reactors. One-dimensional calculations for the corona model of a wire-cylinder reactor showed that fixed ratios of the wire to the cylinder radii, a/b , and the applied voltage to the cylinder radius, V_a/b , were the key design parameters for controlling the discharge characteristics. In addition, shape of pulse voltage externally applied to the electrodes is newly suggested for generating a near-uniform electric field over the entire discharge region. Two-dimensional calculations for a wire-plate reactor found that the wire-to-wire spacing, c , along the parallel-plate direction should be at least twice the wire-to-plate distance, d , to produce non-equilibrium plasmas effectively for generating a large volume of resultant chemically active species ($c/d \geq 2$).

PACS numbers: 52.80.-s, 52.80.Hc

Keywords: Numerical modeling, Corona discharge, Chemically active species, Wire-cylinder reactor, Wire-plate reactor, Geometrical effect

I. INTRODUCTION

The pulsed corona discharge (PCD), which has been widely used for flue gas cleaning and toxic gas decomposition, is one of the most important non-equilibrium plasma sources at atmospheric pressure condition. The PCD generates energetic streamers, which in turn produce numerous chemically active species (CAS), like N, O, and OH in air. The resultant CAS readily destroy hazardous pollutants, such as NO_x (nitrogen oxides) and VOC (volatile organic compounds), by chemical reactions [1–3]. Wire-cylinder and wire-plate types of PCD reactors have been favored due to their simple geometries. However, the non-uniform and time-varying characteristics of streamers make it difficult to analyze and control the flue gas cleaning process by using even simple devices. Therefore, understanding the discharge physics in these reactors is still important for determining the optimal design parameters, such as the wire radius, the wire-to-plate distance, and the neighboring wire distance.

There has been an increasing interest in numerical analysis to find the spatial and the temporal properties of streamers in a variety of corona reactors. One of the

major concerns has been the geometrical configurations of the reactors: for example, pin-plate [4,5], sphere-plate [6], wire-cylinder [7–9], and wire-plate [10,11] geometries. Although some streamer properties have been found in a pin-plate geometry, that geometry has been rather unsuccessful for designing practical corona reactors, such as wire-cylinder and wire-plate reactors, based on this numerical analysis. For wire-cylinder modeling, a 1-D model [7, 8] and a 1.5-D one using a disk method [9] exist. The 1-D model assumes that neighboring streamers are so close to each other that they fill the whole discharge region. This 1-D model can predict streamer properties well near a wire electrode. On the other hand, the 1.5-D model assumes that neighboring streamers are separated far from each other so that a single streamer represents all the streamers with the same physical properties. However, simulation results using the 1.5-D model showed that streamer properties are more affected by the streamer radius, which is an unknown parameter, than by the electrode configuration. Three-dimensional modeling in wire-cylinder and wire-plate reactors should be a good way to consider neighboring streamers realistically. Although we have developed a three-dimensional numerical code and have obtained preliminary results [12], the three-dimensional work still requires numerical improvement.

In this work, considering that the streamer radius is an unknown parameter in the 1.5-D model and that the

*E-mail: yhkim@lanl.gov;

Present address: Plasma Physics Group, Los Alamos National Laboratory, Los Alamos, NM 87545, U.S.A.

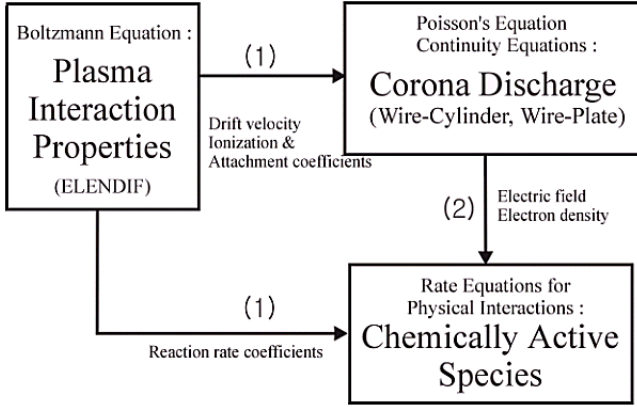


Fig. 1. Three integrated numerical modules for finding the characteristics of corona discharge, the chemically active species, and the plasma interaction properties.

numerical technique in the 3-D model requires improvement, we employed the 1-D model in the wire-cylinder simulation, especially for analyzing the effects of the geometrical configurations of the electrodes on the discharge behavior. The ratio of the wire to cylinder radii and the magnitude of the applied voltage are considered to be crucial parameters influencing streamer propagation. In addition, the present numerical simulations make an attempt to find external pulse voltage waveforms for generating discharge electric fields for effective flue gas cleaning. With an assumption of a negligibly small potential depression in the discharge channel, a unique shape of the pulse voltage is suggested for generating a near-uniform electric field over the whole discharge region of a wire-cylinder reactor. As another important design parameter in 2-D wire-plate modeling, the distance between neighboring wires is taken because narrowing the neighboring wire distance can bring interference effects of discharge fields on streamer propagation.

II. NUMERICAL MODEL AND COMPUTATIONAL METHODS

1. Overview of the Numerical Model

The numerical model, as described schematically in Fig. 1, includes three calculation modules for the corona discharge, the chemically active species (CAS), and the plasma interaction properties. In the corona discharge module, the electric fields and the charged particle densities are computed by solving Poisson's equation and the continuity equations in one or two dimensions. The calculated plasma variables are then used as inputs for the CAS module, where the densities of several CAS are calculated by taking into account a set of rate equations for electron interactions with air molecules. Meanwhile, the transport and the collision coefficients are required for

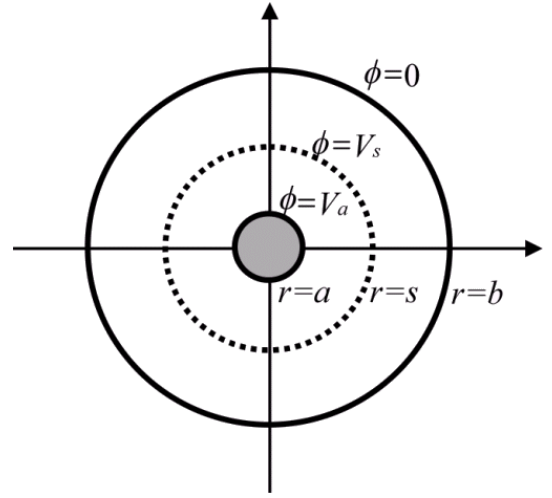


Fig. 2. Computational domain of a wire-cylinder PCD reactor. A dotted circle at $r = s$ illustrates the propagating streamer front.

self-consistent calculations of the corona and the CAS modules. In this work, the Boltzmann equation solver ELENDIF [13] is adopted to calculate the transport and interaction properties as a function of the electric field in the range of 5 ~ 200 kV/cm.

2. Corona Discharge Model in a Wire-Cylinder Geometry

The computational domain of the wire-cylinder PCD reactor is presented in Fig. 2. A positive voltage V_a is applied to a wire anode of radius a while the outer cylinder tube of radius b is grounded. Positive streamers are initiated at the surface of the wire anode and propagate toward the grounded outer cathode. It is assumed that many streamers take place symmetrically at the same time and that the neighboring streamers are so close to fill the whole discharge region. In Fig. 2, the instantaneous location of the propagating streamer front is represented as a dotted circle at $r = s$.

In this 1-D corona model, the propagating streamers depend on the radial direction in cylindrical coordinates. The following are the governing equations describing the corona discharge in the wire-cylinder geometry [7,9]:

$$\frac{d^2\phi}{dr^2} + \frac{1}{r} \frac{d\phi}{dr} = -\frac{e}{\epsilon_0} (n_p - n_e - n_n), \quad (1)$$

$$\frac{\partial n_e}{\partial t} + \frac{1}{r} \frac{\partial}{\partial r} (r n_e v_{de}) = (1 + \gamma_{ph}) \alpha n_e |v_{de}| - \beta n_e |v_{de}|, \quad (2)$$

$$\frac{\partial n_p}{\partial t} + \frac{1}{r} \frac{\partial}{\partial r} (r n_p v_{dp}) = (1 + \gamma_{ph}) \alpha n_e |v_{de}|, \quad (3)$$

$$\frac{\partial n_n}{\partial t} + \frac{1}{r} \frac{\partial}{\partial r} (r n_n v_{dn}) = \beta n_e |v_{de}|. \quad (4)$$

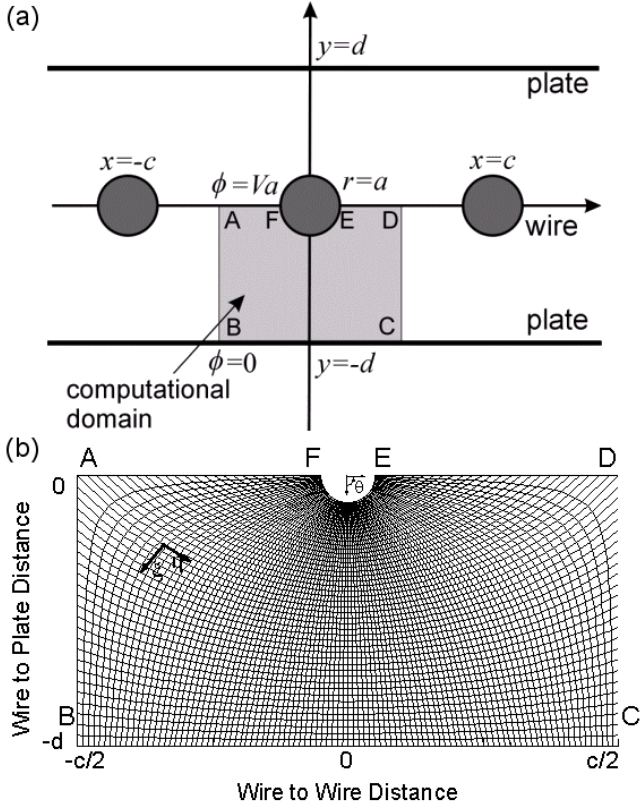


Fig. 3. (a) Computational domain of a wire-plate PCD reactor and (b) its numerical grid system with 50×100 nodes.

Here, ϕ is the electric potential in units of [V], e is the electric charge of 1.6×10^{-19} C, and ϵ_0 is the electric permittivity of 8.854×10^{-14} C/cm² for air. The ambient gas is assumed to be $N_2/O_2/H_2O/CO_2 = 74.1/3.3/8.3/14.3$. Positive ions include N_2^+ , O_2^+ , H_2O^+ , and CO_2^+ . The total number density of positive ions is represented by n_p . The total number density of negative ions, which include O^- , O_2^- , H^- , and OH^- , is represented by n_n , and the number density of electrons is n_e . v_{de} , v_{dp} , and v_{dn} are the drift velocity of the respective plasma species. The right-hand sides of Eqs. (2) ~ (4) represent the source terms of each charged species. γ_{ph} is the photo-ionization coefficient in air, for which the experimental value given by Penny and Hummert [14] was used in the present numerical work. α is the total ionization coefficient, and β is the total attachment coefficient. The boundary values of the electric potential at the two electrodes are

$$\phi = V_a \text{ at the anode, } \phi = 0 \text{ at the cathode.} \quad (5)$$

The boundary conditions for the charged particles den-

sity, n , are

$$\left. \frac{\partial n}{\partial r} \right|_{r=a} = \left. \frac{\partial n}{\partial r} \right|_{r=b} = 0. \quad (6)$$

Poisson's equation, Eq. (1), is solved by a SOR (successive over relaxation) scheme. For solving Eqs. (2) ~ (4), we employed the flux corrected transport (FCT) algorithm suggested by Zalesak [15]. The upwind and Lax-Wendroff methods are used as low- and high-order schemes of the FCT algorithm, respectively [16].

3. Corona Discharge Model in a Wire-Plate Geometry

Figure 3(a) presents a cross-sectional view of the wire-plate PCD reactor, in which the computational domain is shaded. Three representative wire electrodes are placed at $x = 0, c,$ and $-c$, respectively, along the parallel-plate direction. All the wire electrodes have the same radius a and the same applied potential V_a . The two grounded plates are located at $y = d$ and $-d$, respectively. The rectangular coordinate system (x, y) is transformed into curvilinear coordinates (ξ, η) to handle the curved surface of the wire electrode effectively. A curvilinear numerical grid system is generated by means of the two-dimensional elliptic partial-differential-equation method [16,17]:

$$\nabla^2 x = 0 \rightarrow h_\eta^2 \frac{\partial^2 x}{\partial \xi^2} - 2h_{\xi\eta} \frac{\partial^2 x}{\partial \xi \partial \eta} + h_\xi^2 \frac{\partial^2 x}{\partial \eta^2} = 0, \quad (7)$$

$$\nabla^2 y = 0 \rightarrow h_\eta^2 \frac{\partial^2 y}{\partial \xi^2} - 2h_{\xi\eta} \frac{\partial^2 y}{\partial \xi \partial \eta} + h_\xi^2 \frac{\partial^2 y}{\partial \eta^2} = 0, \quad (8)$$

where the h_ξ , h_η , and $h_{\xi\eta}$ are metric coefficients. Figure 3(b) shows a numerically generated grid with 50×100 nodes, where θ is the value of the angle from the y -axis to the x -axis. Based on the curvilinear grid generation, the above number of grids is used for all wire-plate calculations, regardless of the value of $a, c,$ and d .

The Poisson's equation transformed into the (ξ, η) coordinates is

$$\frac{1}{J} \frac{\partial}{\partial \xi} \left(\frac{h_\eta^2}{J} \frac{\partial \phi}{\partial \xi} \right) - \frac{2}{J} \frac{\partial}{\partial \xi} \left(\frac{h_{\xi\eta}}{J} \frac{\partial \phi}{\partial \eta} \right) + \frac{1}{J} \frac{\partial}{\partial \eta} \left(\frac{h_\xi^2}{J} \frac{\partial \phi}{\partial \eta} \right) = 0. \quad (9)$$

Here, $J = \frac{\partial x}{\partial \xi} \frac{\partial y}{\partial \eta} - \frac{\partial y}{\partial \xi} \frac{\partial x}{\partial \eta}$ is the Jacobian of the (ξ, η) coordinates. The continuity equations of the charged particles density are expressed as

$$\frac{\partial n_e}{\partial t} + \frac{1}{J} \frac{\partial}{\partial \xi} \left(\frac{J}{h_\xi} n_e v_{de}^\xi \right) + \frac{1}{J} \frac{\partial}{\partial \eta} \left(\frac{J}{h_\eta} n_e v_{de}^\eta \right) = (\alpha - \beta) n_e |v_{de}|, \quad (10)$$

$$\frac{\partial n_p}{\partial t} + \frac{1}{J} \frac{\partial}{\partial \xi} \left(\frac{J}{h_\xi} n_p v_{dp}^\xi \right) + \frac{1}{J} \frac{\partial}{\partial \eta} \left(\frac{J}{h_\eta} n_p v_{dp}^\eta \right) = \alpha n_e |v_{de}|, \quad (11)$$

$$\frac{\partial n_n}{\partial t} + \frac{1}{J} \frac{\partial}{\partial \xi} \left(\frac{J}{h_\xi} n_n v_{dn}^\xi \right) + \frac{1}{J} \frac{\partial}{\partial \eta} \left(\frac{J}{h_\eta} n_n v_{dn}^\eta \right) = \beta n_e |v_{de}|. \quad (12)$$

The following boundary conditions are used in the wire-plate geometry. At the boundary (AB, CD),

$$\xi_x \frac{\partial \phi}{\partial \xi} + \eta_x \frac{\partial \phi}{\partial \eta} = 0, \quad (13)$$

$$\xi_x \frac{\partial n}{\partial \xi} + \eta_x \frac{\partial n}{\partial \eta} = 0. \quad (14)$$

At the boundary (BC),

$$\phi = 0, \quad (15)$$

$$\xi_x \frac{\partial n}{\partial \xi} + \eta_x \frac{\partial n}{\partial \eta} = 0. \quad (16)$$

At the boundary (DE, FA),

$$\xi_y \frac{\partial \phi}{\partial \xi} + \eta_y \frac{\partial \phi}{\partial \eta} = 0, \quad (17)$$

$$\xi_y \frac{\partial n}{\partial \xi} + \eta_y \frac{\partial n}{\partial \eta} = 0. \quad (18)$$

At the boundary (EF),

$$\phi = V_a, \quad (19)$$

$$\left(\xi_x \frac{\partial n}{\partial \xi} + \eta_x \frac{\partial n}{\partial \eta} \right) \cos \theta + \left(\xi_y \frac{\partial n}{\partial \xi} + \eta_y \frac{\partial n}{\partial \eta} \right) \sin \theta = 0. \quad (20)$$

For solving these equations by the finite difference method (FDM), we used a conjugate gradient scheme for Poisson's equation and an upwind scheme for the continuity equations.

4. Generation of Chemically Active Species

Chemically active species (CAS) can be classified into two groups: i) primary CAS created by electron-impact processes of ambient neutral molecules and ii) secondary CAS generated by the primary CAS reacting with neutral molecules. In this CAS numerical module, however, only the primary CAS are considered because the calculation time is relatively short to produce secondary CAS. The ambient air includes nitrogen, oxygen, water vapor, and carbon dioxide. Table 1 lists the several physical interactions taken into account in this CAS module.

The concentration n_x of CAS x is calculated by the rate equations [4]

$$\frac{dn_x}{dt} = \sum_j ck_{xj} n_e n_m, \quad (21)$$

where c is the stoichiometric coefficient, k_{xj} is the reaction rate coefficient, and n_m is the concentration of parent molecules of the product x in each interaction. There are 13 reaction products: N₂(A), N, O₂(a), O, O(¹D), OH, H, CO, e, N₂, O₂, H₂O, and CO₂. For convenience, O(³P) is represented by O in this work. The reaction rate coefficients, $k_1 \sim k_7$, are obtained from the plasma properties module. For the simultaneous computations involving Eqs. (21), the electric field and the electron density calculated from the plasma module are used. When calculating the coupled ordinary differential equations in Eqs. (21), we used an explicit Euler scheme. Although the large differences in the reaction rate coefficients make Eqs. (21) stiff, use of a short time step of 10⁻¹¹ sec produced in the reliable calculations.

5. Determination of the Plasma Properties

The plasma interaction properties, including the transport and the collision coefficients, depend on the electron energy distribution function (EEDF). For their calculations, a Boltzmann solver ELENDIF [13] is used in this numerical work. Several inelastic collisions by electrons with neutrals, such as excitation, ionization, attachment, and dissociation, can be represented on the basis of Krook's collision model [13]. Since ELENDIF requires cross-section values as input data, the JILA (Joint

Table 1. Electron impact interactions with ambient air molecules considered in the CAS module.

Ambient gas	Reactions	Rate coeffi.
Nitrogen	$e + \text{N}_2 \rightarrow \text{N}_2(\text{A}) + e$	k_1
	$e + \text{N}_2 \rightarrow \text{N} + \text{N} + e$	k_2
Oxygen	$e + \text{O}_2 \rightarrow \text{O}_2(\text{a}) + e$	k_3
	$e + \text{O}_2 \rightarrow \text{O} + \text{O} + e$	k_4
	$e + \text{O}_2 \rightarrow \text{O}(\text{1D}) + \text{O} + e$	k_5
Water vapor	$e + \text{H}_2\text{O} \rightarrow \text{OH} + \text{H} + e$	k_6
Carbon dioxide	$e + \text{CO}_2 \rightarrow \text{CO} + \text{O} + e$	k_7

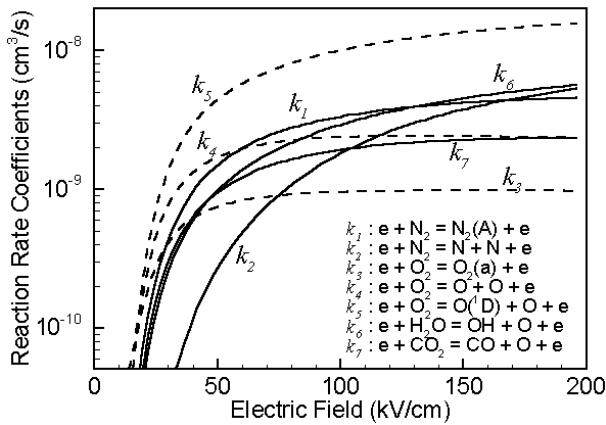


Fig. 4. Various reaction rate coefficients caused by electron collisions with molecules in air as functions of the electric field ($N_2/O_2/H_2O/CO_2 = 74.1/3.3/8.3/14.3$).

Institute of Laboratory Astronomy) database was compiled for nitrogen, oxygen, water vapor, and carbon dioxide.

Once the EEDF, f , is found, the plasma interaction properties can be derived as a function of the electron energy, ϵ . Local field equilibrium is well known to be satisfied at atmospheric pressure. This means that f and the corresponding plasma properties are only functions of E/N , where E is the total electric field and N is the background neutral density [18]. The interaction rate coefficients, k , caused by electron collisions with the molecules in air are also computed by the ELENDIF through

$$k = \langle \sigma v \rangle_f = \int_0^\infty \sigma v f(\epsilon) d\epsilon, \quad (22)$$

where σ is the collision cross-section for the corresponding interaction with an electron, and v is the relative velocity between electrons and molecules. The calculated rate coefficients for various interactions by electron collisions with molecules in air are plotted in Fig. 4.

III. RESULTS AND DISCUSSION

1. 1-D Modeling of a Wire-Cylinder Reactor

A. Streamer Propagation and CAS Generation

In wire-cylinder modeling, the radii of the anode wire and the cathode cylinder are set to be 0.2 and 2.0 cm, respectively. A constant voltage of 46 kV is applied to the anode wire. A spatially uniform electron distribution of 1 cm^{-3} is used as an initial condition. A grid size of 10^{-3} cm and a time step of 10^{-11} sec are taken for the calculations.

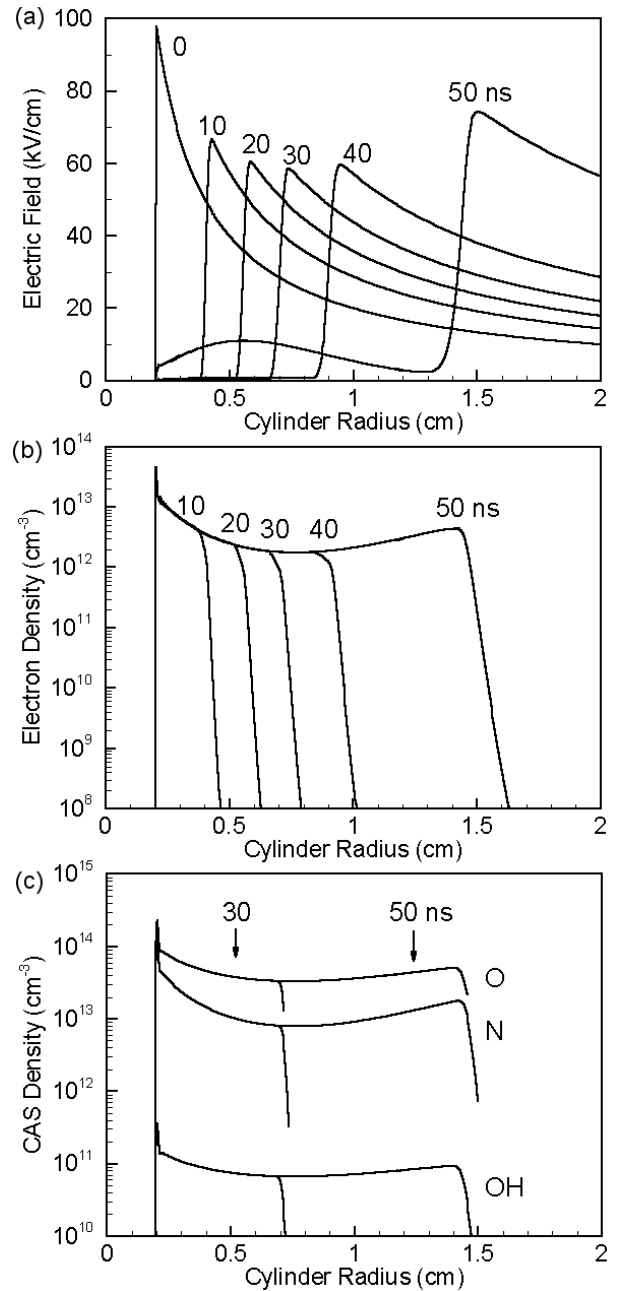


Fig. 5. Radial profiles of (a) the electric field, (b) the electron density, and (c) the densities of the CAS during positive streamer propagation in a wire-cylinder PCD reactor ($a = 0.2 \text{ cm}$, $b = 2 \text{ cm}$, $V_a = 46 \text{ kV}$).

Figure 5(a) shows the radial profiles of electric fields during streamer propagation. An initial maximum electric field of 100 kV/cm at the wire anode surface ($r = a$) decreases to about 60 kV/cm at a streamer front during 40 ns. As the streamer front at $r = s$ moves toward the cylinder electrode ($r = b$), the electric field becomes nearly zero inside the streamer channel ($a < r < s$) and is pushed out beyond the streamer region ($s < r < b$). The numerically calculated electric field at $r = a$ was

compared with analytical one. In wire-cylinder geometry, the vacuum electric field at the wire surface ($r = a$) is determined by [19]

$$E(a) = \frac{-V}{\ln(a/b)} \frac{1}{a}, \quad (23)$$

where a is the radius of the wire electrode, b is the radius of the cylinder electrode, and V is the applied voltage. For example, if $a = 0.2$ cm, $b = 2$ cm, and $V = 46$ kV, then the analytical $E(a)$ is 100 kV/cm, which is consistent with the numerically calculated one.

Shown in Figure 5(b) are the radial density profiles of electrons generated during positive streamer propagation. The calculated electron densities in the wire-cylinder reactor are in the range of $2 \times 10^{12} \sim 10^{13}$ cm $^{-3}$. The spatial profiles of the electron density are observed to trace the streamer front propagation because electrons are produced dominantly near the streamer front and because the negligible drift velocity in the streamer channel causes the electron to remain in the region between the wire anode and the streamer front.

Figure 5(c) shows that the spatial-temporal density distributions of CAS produced in air during streamer propagation. In this figure, the CAS density profiles follow the electron profile, but the magnitudes of the CAS concentrations depend on their reaction rate coefficients. O atoms turn out to be the most abundant radicals, ranging from 3×10^{13} to 10^{14} cm $^{-3}$ in these conditions. On the other hand, OH species are generated in the range of about 10^{11} cm $^{-3}$.

B. Effects of Reactor Geometry on Plasma Generation

For the wire-cylinder geometry, as with the previous simulation, the effects of the applied DC voltage level V_a on plasma generation are examined. For four levels of applied voltage, $V_a = 37, 41, 46,$ and 55 kV, the calculated results are illustrated in Fig. 6(a) by tracing the electric field peak values of the moving streamer at its head. When 37-kV DC is applied between the wire and the cylinder electrodes, the corresponding streamer ceases to propagate near the wire electrode (at 0.5 cm). As long as the applied voltage is greater than 41 kV, the streamer propagates covering the whole region of this reactor and can be called a bridged streamer. This 41 kV might be determined as the onset voltage for a bridged streamer in this wire-cylinder geometry ($a = 0.2$ and $b = 2$ cm). Unfortunately, values of the onset field or voltage for a bridged streamer are not available in the literature. However, the partial-breakdown condition [such as line (1) in Fig. 6(a)] has been investigated for various types of geometries. For instance, in 1929, Peek [19] experimentally found the partial-breakdown field, E_c , of air in a wire-cylinder geometry to be

$$E_c = 31 \left(1 + \frac{0.308}{\sqrt{a}} \right) \text{ [kV/cm]}. \quad (24)$$

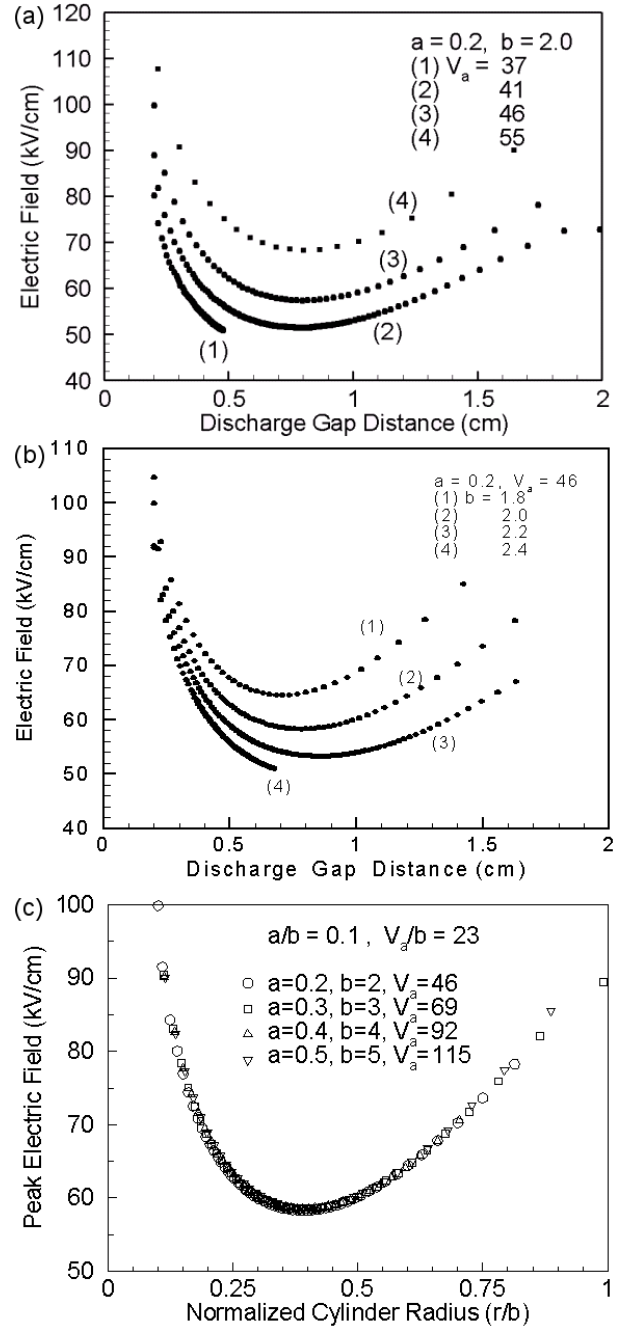


Fig. 6. Effects of (a) the DC voltage level, (b) the cylinder radius, and (c) different values of $a, b,$ and V_a constrained such that $a/b = 1$ and $V_a/b = 23$ on the propagation characteristics of streamers in a wire-cylinder PCD reactor.

According to Eq. (24), E_c requires about 52 kV/cm for $a = 0.2$ cm. Whenever the maximum electric field $E(a)$ is greater than the partial-breakdown field E_c , a streamer will be generated. Let $E(a) > E_c$, then, the streamer onset voltage corresponding to the partial-breakdown volt-

age is found from

$$V_b \geq -31 \left(1 + \frac{0.308}{\sqrt{a}} \right) a \ln \left(\frac{a}{b} \right) \quad [kV]. \quad (25)$$

For example, if a wire-cylinder reactor has $a = 0.2$ cm and $b = 2$ cm, the V_b is estimated to be 24 kV. In this numerical calculation, partial breakdown was observed at 24 ~ 41 kV. The bridged streamer occurred at 41 kV, as shown in Fig. 6(a).

Next, the effect of the discharge gap on plasma generation is calculated in a wire-cylinder reactor with a wire radius of 0.2 cm and an applied DC voltage of 46 kV. Four different radii of the cylinder electrode are used, *i.e.*, $b = 1.8, 2.0, 2.2,$ and 2.4 cm. The calculated results are drawn in Fig. 6(b) for the peak traces of the electric field of the moving streamer head. When the cylinder radius becomes larger, the streamer has a lower electric field and stops propagating under a certain value of the cylinder radius because the internal electric field reduces with enlarging outer cylinder electrode.

After investigating the influences of the discharge operating parameters on plasma generation, we determined dominant parameter for the wire-cylinder reactor. The maximum vacuum electric field at $r = a$ is given by

$$E(a) = \frac{-V_a}{a \ln(a/b)} = \frac{-(V_a/b)}{(a/b) \ln(a/b)}. \quad (26)$$

Here, a is the radius of the wire electrode, b is the radius of the cylinder electrode, and V_a is the applied voltage. From this equation, the maximum electric field at the wire surface ($r = a$) can be analytically expressed as functions of the wire radius to cylinder radius ratio (a/b) and the applied voltage to the cylinder radius ratio (V_a/b). However, Eq. (26) is satisfied only at the surface of the wire electrode before a breakdown of the corona discharge, so numerical simulations are needed to verify whether these parameters, a/b and V_a/b , can affect the propagation characteristics of streamers.

Four calculating conditions are considered in this simulation. In each case, a , b , and V_a are varied with fixed values of $a/b = 0.1$ and $V_a/b = 23$ kV/cm. The traces of the electric field at the moving streamer front are plotted in Fig. 6(c) as a function of the normalized cylinder radius (r/b). The initial electric field at the wire electrode is 100 kV/cm for each case. During the discharge, the streamers generated in the four different types of the wire-cylinder reactors show the same propagation characteristics. This implies that the same discharge properties can be expected whenever a/b and V_a/b are maintained with their respective ratios. Consequently, from these simulation results, the parameters a/b and V_a/b are found to play a key role in the control of streamer discharges in wire-cylinder PCD reactors.

C. Pulse Voltage Waveform Generating a Near-Uniform Electric Field

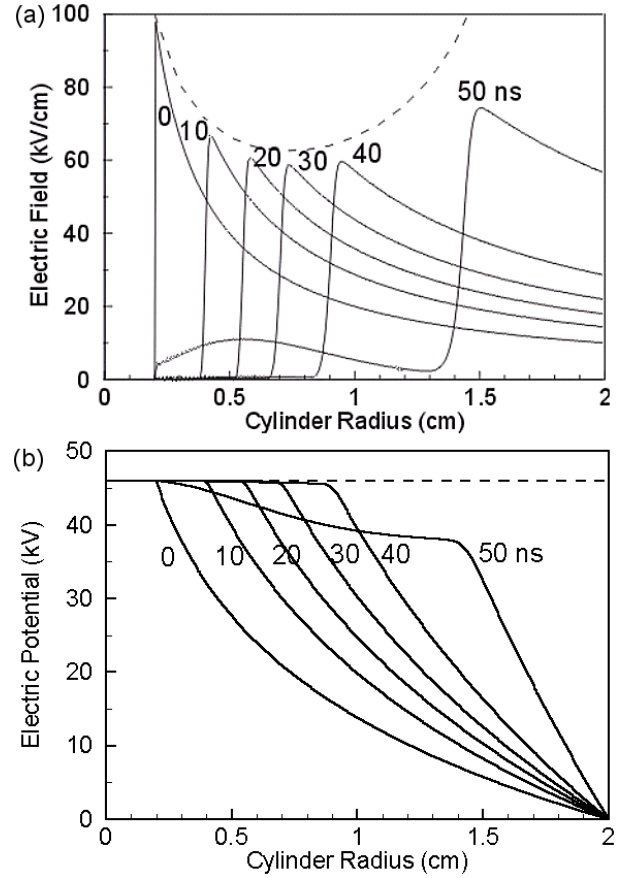


Fig. 7. Numerical (solid line) and analytical (Eq. (27), dashed line) results for the radial profiles of (a) the electric field and (b) the electric potential during positive streamer propagation in a wire-cylinder PCD reactor ($a = 0.2$ cm, $b = 2$ cm, $V_a = 46$ kV).

Uhm and Lee's analytical work suggested that the electrical potential depression in the streamer channel is negligibly small due to the high conductivity of the streamer channel [20], which implies that streamers have a role to expand virtually the radius of the wire electrode and that the streamer plasma can be treated approximately as a cylindrical conductor. In this case, the electric field in the streamer channel ($a < r < s$) is zero, and the electric field at the streamer front s can then be expressed as

$$E(s) = \frac{-V_s}{s \ln(s/b)}, \quad (27)$$

where a in Eq. (23) has been replaced with s . V_s is the voltage at the streamer front, which is maintained at the same potential as the externally applied voltage, V_a , to the wire anode ($V_s \approx V_a$). In this numerical work, it is quite meaningful to compare numerically calculated results with the previous analytical description to examine the validity of Eq. (27) and to get efficient voltage waveforms for effective CAS generation.

In Fig. 7(a), the numerical results for the electric field (solid line) are compared with the analytical description

(dashed line) represented by Eq. (27). As Fig. 7(a) shows, the numerical and the analytical results are in quite good agreement within the upstream channel region (< 1 cm), where the ideal assumption of a cylindrical conductor is applicable to the channel in the theory. However, the differences increase as the streamer front approaches the cylinder cathode, where the potential depression increases as the streamer channel elongated. Figure 7(b) displays the calculated electrical potential profiles corresponding to Fig. 7(a). As expected, the potential depression in the channel is negligible in the early stage of the corona discharge (< 40 ns), but it steadily increases as the streamer approaches the cylinder cathode.

In a comparison of streamer propagation at constant voltage, the applied pulse voltage profile V_a sustaining the streamer with uniform peak electric fields is deduced from Eq. (27) as

$$V_a \approx V_s = -s \ln(s/b)E(s). \quad (28)$$

If we put $E(s)$ as 24 kV/cm to maintain the streamer onset voltage for atmospheric-pressure air breakdown, the sustained voltage at the streamer front is then $V_s[\text{kV}] = -24 s \ln(s/b) = V_c$, where V_c is defined, for convenience, as the critical applied pulse voltage for air breakdown.

In Fig. 8(a), V_c is plotted with dashed line as a function of the location of the propagating streamer front. Three cases of $V_s/V_c = 2.5, 3.0,$ and 3.5 are considered for the simulation of streamer propagation in the wire-cylinder reactor. These pulse voltages have a parabolic shape as a function of the streamer front location s . When the streamer front location is near the wire electrode, the rising pulse voltage in Fig. 8(a) will compensate for the decreasing tendency of electric field, shown at a constant-voltage simulation in Fig. 7(a). On the other hand, the falling phase of the pulse voltages in Fig. 8(a) can reduce the increasing electric field near the cylinder electrode. Simulation results for the voltage of the streamer front, V_s , are also shown as symbols in Fig. 8(a). In comparison to the analytical approximation, potential depressions ($V_a - V_s$) are observed for three simulations. The simulation results in Fig. 8(b) indicate that the traces of streamer fronts traveling toward the cylinder cathode exhibit nearly uniform distributions of their electric fields in the discharge region. The peak electric fields increase with the applied pulse voltage level. From this calculation, the applied voltage profiles along the streamer front positions in the discharge reactor can be converted to voltage pulse waveforms in the time domain. If the calculated streamer velocity v at the position s is used, the pulse voltage waveforms are found as $V_a(t) \approx V_s(t) \propto -(vt) \ln((vt)/b)$. In Fig. 8(c), the calculated voltage pulse waveforms required to produce near-uniform electric fields are shown for $V_s/V_c = 2.5, 3.0,$ and 3.5 as functions of time. The applied pulse width is noticed to considerably lessen from 120 ns to 20 ns as the applied voltage V_s is increased from $2.5 V_c$ to $3.5 V_c$. Since these external pulse waveforms can pro-

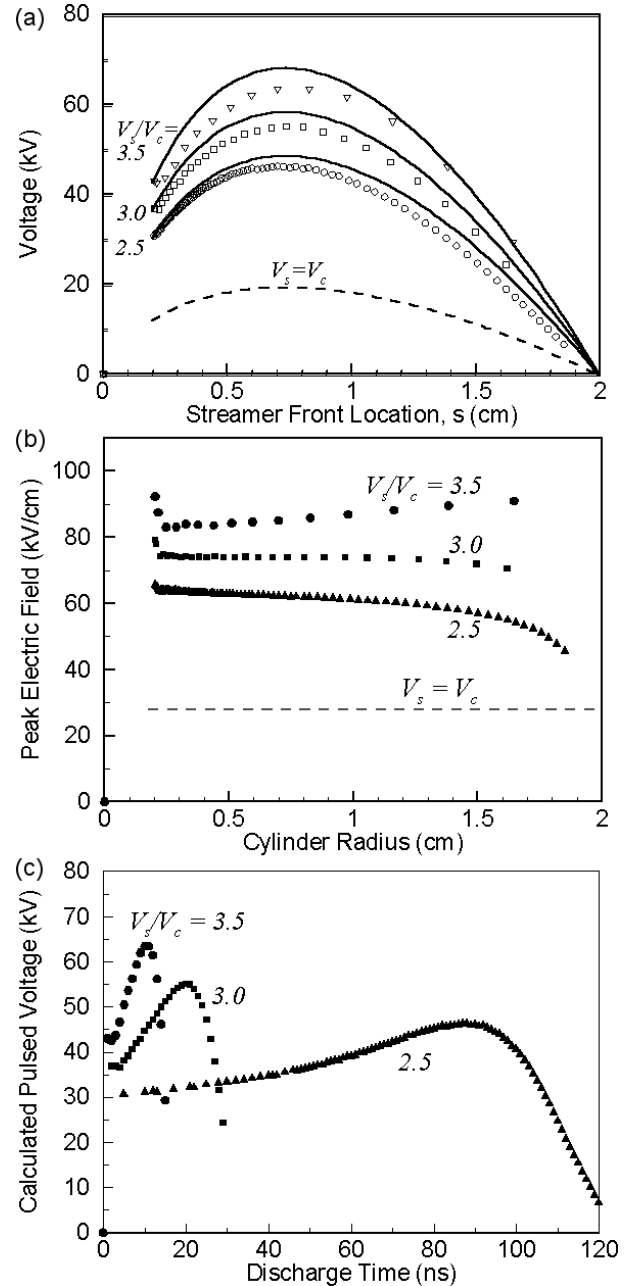


Fig. 8. (a) Voltage profiles applied to the wire electrode (solid lines) and simulation results for the voltages at the streamer front (symbols). (b) Peak electric field distributions of the streamers obtained by using the applied voltage profiles of (a). (c) Resultant voltage pulse waveforms required to produce the near-uniform electric fields shown in (b) as functions of time.

duce near-uniform electric fields, primary CAS can also be generated uniformly, even in a wire-cylinder reactor. Moreover, we can selectively control the density of a certain CAS, such as O or N, because it mainly depends on the electric field at the streamer front.

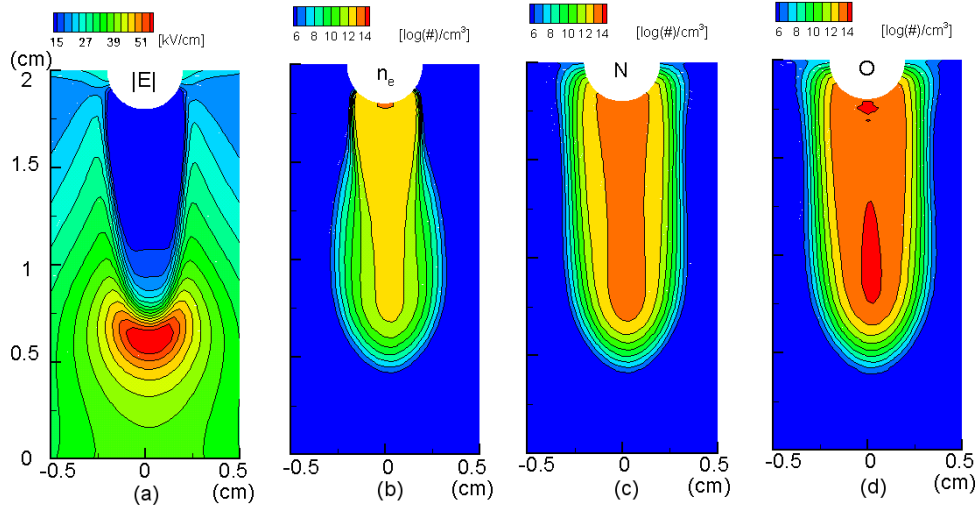


Fig. 9. Propagation images of (a) the electric field, (b) the electron density, (c) the N-radical density, and (d) the O-radical density along the streamer channel at 30 ns after streamer generation in a wire-plate reactor ($b = 2$ cm, $c = 4$ cm, $V_a = 46$ kV).

2. 2-D Modeling of a Wire-Plate Reactor

A. Streamer Propagation and CAS Generation

In wire-plate modeling, the radius a of the anode wire is 0.2 cm, and the distance d between the center of the wire and the cathode plate is 2 cm. The neighboring wire distance c is set to 4 cm. The geometrical arrangement used in this calculation can be characterized as $a/d = 0.1$ and $c/d = 2$. An external constant voltage of 46 kV is applied to the anode wire, and a spatially uniform electron distribution of 1 cm^{-3} is used as an initial condition. A numerical grid with 50×100 nodes and a time step of 10^{-12} sec are used for the calculations.

Figure 9 illustrates the calculated 2-D distributions of (a) the electric field intensity, (b) the electron density, (c) the N species, and (d) the O species along the streamer channel at 30 ns after streamer generation. A positive streamer initiated by air breakdown at the anode wire surface propagates toward the grounded cathode plate to form a discharge channel with an electron density of 10^{13} cm^{-3} . The initial non-uniform electric field, with maximum value of 78 kV/cm, gradually reduces to about 55 kV/cm as the polarization field is formed by net space charges produced by the different drift velocities between electrons and ions. The 2-D distributions of CAS are also obtained and are shown in Fig. 9(c), where N species are mainly generated around the streamer front due to the higher electric field needed for nitrogen molecule dissociations. On the other hand, the O species in Fig. 9(d) require less electron energy and exist in the streamer channels with lower electric fields.

B. Neighboring Wire Effect

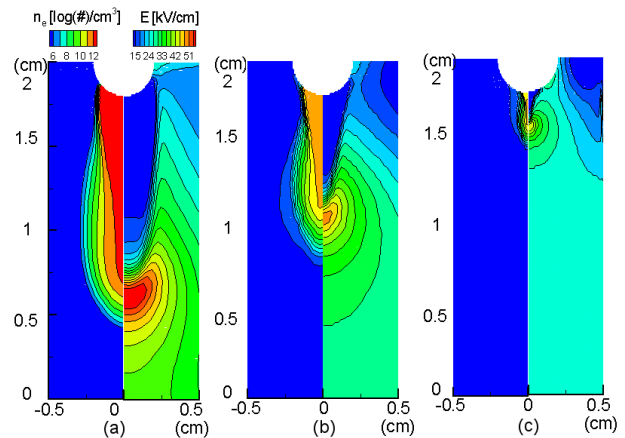


Fig. 10. Propagation images of the electron density (left) and the electric field intensity (right) at 30 ns after streamer generation in a wire-plate reactor ($b = 2$ cm, $V_a = 46$ kV) for wire-to-wire distances of (a) $c = 4$ cm, (b) $c = 2$ cm, and (c) $c = 1$ cm.

In order to investigate the influence of the neighboring wire distance on the streamer propagation, we carried out simulations for different wire-to-wire distances of (a) $c = 4$ cm, (b) $c = 2$ cm, and (c) $c = 1$ cm. Since $d = 2$ cm, the respective ratios of wire-to-wire spacing to wire-to-plate distance are (a) $c/d = 2$, (b) $c/d = 1$, and (c) $c/d = 0.5$. As Fig. 10 shows, as the adjacent wire electrodes are brought closer, their interference effects on the electric field distributions become stronger, and the streamers from the adjacent wires, consequently, shrink up to considerably narrow ranges. Although the same voltage is applied in all three cases, the closer arrangement of the neighboring wires brings about reductions in the electron density and the electric field in the streamer front. Generation of CAS is also affected by the elec-

trode arrangement in the wire-plate reactor. We, therefore, conclude that the wire-to-wire spacing should be at least twice the wire-to-plate distance ($c/d \geq 2$) to produce an effective non-equilibrium plasma for enhancing the efficiency of the flue gas cleaning process.

IV. CONCLUSIONS

Time-dependent one- and two-dimensional numerical codes are developed for wire-cylinder and wire-plate PCD reactors. Three calculation modules are employed for (1) the corona discharges, (2) the chemically active species, and (3) the plasma interaction properties using the Boltzmann equation solver ELENDF. Simulations are mainly focused on finding the governing design parameters of two corona discharge reactors.

In the wire-cylinder reactor, the maximum electric field at the wire surface can be analytically expressed as functions of the ratio of the wire to the cylinder radii, a/b , and the ratio of the applied voltage to the cylinder radius, V_a/b . Numerical simulations also reveal that propagating streamers are governed by the two parameters a/b and V_a/b , which implies that the same discharge properties can be expected whenever a/b and V_a/b are maintained at their respective ratios. In order to control the electric field at the propagating streamer front, we carried out numerical calculations to determine the pulse voltage waveforms for effective flue gas cleaning. With an assumption of negligibly small potential depression in the streamer channel, an optimum pulse voltage shape of $V_s \propto -s \ln(s/b)$ is suggested for generating a near-uniform electric field over the whole discharge region.

In the wire-plate reactor, curvilinear coordinates are employed to handle realistically the geometry of the wire-plate reactor. As the adjacent wire electrodes are brought closer, their interference effects on the electric field distributions become stronger, so the streamers shrink up to considerably narrow ranges. Two-dimensional calculations have found that the wire-to-wire spacing, c , should be at least twice the wire-to-plate distance, d , to produce a non-equilibrium plasma that is

effective for generating many chemically active species ($c/d \geq 2$).

REFERENCES

- [1] R. Hackam and H. Akiyama, IEEE Trans. Die. Elect. Insul. **7**, 654 (2000).
- [2] L. A. Rosocha and R. A. Korzekwa, J. Adv. Oxid. Technol. **4**, 247 (1999).
- [3] Y. Kim, W. S. Kang, J. M. Park, S. H. Hong, Y. H. Song and S. J. Kim, IEEE Trans. Plasma Sci. **32**, 18 (2004).
- [4] A. A. Kulikovskiy, IEEE Trans. Plasma Sci. **25**, 439 (1997).
- [5] R. Morrow and J. J. Lowke, J. Phys. D: Appl. Phys. **30**, 614 (1997).
- [6] W. S. Kang, J. M. Park, Y. Kim and S. H. Hong, IEEE Trans. Plasma Sci. **31**, 504 (2003).
- [7] S. T. Chun, J. Korean Phys. Soc. **33**, 428 (1998).
- [8] W. H. Koh and I. H. Park, J. Korean Phys. Soc. **42**, S920 (2003).
- [9] Y. L. M. Creyghton, Ph.D. dissertation, Eindhoven University of Technology, Eindhoven, The Netherlands, 1994.
- [10] I. Gallimberti, J. Electrostatics **43**, 219 (1998).
- [11] Y. Kim and S. H. Hong, IEEE Trans. Plasma Sci. **30**, 168 (2002).
- [12] J. M. Park, Y. Kim and S. H. Hong, *Proceedings of the 8th Int. Sym. High Pressure Low Temperature Plasma Chemistry* (Puhajarve, Estonia, 2002), Vol. 1, p. 104.
- [13] W. L. Morgan and B. M. Penetrante, Comp. Phys. Comm. **58**, 127 (1990).
- [14] G. W. Penny and G. T. Hummert, J. Appl. Phys. **41**, 572 (1970).
- [15] S. T. Zalesak, J. Comput. Phys. **31**, 335 (1979).
- [16] K. A. Hoffman, *Computational Fluid Dynamics for Engineers* (EES, Austin, 1989), Chap. 6.
- [17] W. D. D'haeseleer, W. N. G. Hitchon, J. D. Callen and J. L. Shohet, *Flux Coordinates and Magnetic Field Structure* (Springer-Verlag, Berlin, Germany, 1991).
- [18] J. J. Lowke and D. K. Davies, J. Appl. Phys. **48**, 4991 (1977).
- [19] Y. P. Raizer, *Gas Discharge Physics* (Springer-Verlag, Berlin, Germany, 1991), Chap. 12.
- [20] H. S. Uhm and W. M. Lee, Phys. Plasmas **4**, 3117 (1997).